A THREE-DIMENSIONAL THERMAL-HYDRO-MECHANICAL-CHEMICAL BOND CONTACT MODEL FOR METHANE HYDRATE BEARING SEDIMENTS

Mingjing Jiang[1], Ruohan Sun[2] and Wenhao Du[3]

[1] Department of Civil Engineering, College of Civil Engineering, Tianjin University
Tianjin 300072
E-mail :mingjing.jiang@tju.edu.cn

[2] Department of Civil Engineering, College of Civil Engineering, Tianjin University
Tianjin 300072
E-mail :sunruohan@tju.edu.cn

[3]Department of Geotechnical Engineering, College of Civil Engineering, Tongji University
Shanghai 200092
E-mail : 1530405@tongji.edu.cn

Keywords Methane hydrate-bearing sediment, DEM, THMC bond contact model, Mechanical behaviour

Abstract It is well known that the mechanical properties of Methane Hydrate-Bearing Sediments (MHBS) are complex and highly influenced by the surrounding temperature, pore pressure, effective stress and salinity. This paper proposes a three-dimensional(3D) bond contact model which incorporates the effects of temperature, pore pressure, effective stress and salinity. The model is then implemented in a distinct element method(DEM) code which can be employed for thermal–hydro–mechanical-chemical (THMC) analysis. The mechanical behaviour of MHBS was investigated by simulating a series of triaxial compression tests on MHBS with various MH saturations , effective confining pressures and salinity. The results show that the DEM with the proposed contact model is able to capture the salient properties of MHBS, such as the effects of hydrate saturation, effective confining pressure and salinity. The numerical results show that: the shear strength and secant modulus increase as the methane hydrate saturation or effective confining pressure increases, which are in good agreement with the experimental observation. The peak shear strength decreases significantly while the residual shear strength decreases slightly with the increase of salinity.

1 INTRODUCTION

Methane Hydrate (MH, also named natural gas hydrate), is a cage-like crystalline solid[1] which is recognized as a potential new energy in the future. The sediment containing MH is usually referred as the Methane Hydrate-Bearing sediments (MHBS)[2]. Due to their potential use as a future energy source, the MHBS have attracted many researches on the physical, chemical and mechanical properties.

Currently, the understanding of the mechanical properties of MHBS still remains in the accumulation stage of basic experimental data. The existing laboratory tests mainly focus on the mechanical properties of MHBS, and the effect of temperature, MH saturation, confining pressure and backpressure. However, few attention was paid on effect of the chemical conditions, which constitutes one of our motivations in this study.

The Discrete Element Method (DEM)[3], which takes particles as the basic unit and can

well present the microscopic properties of particle materials, has been widely used in the research of MHBS. The key point of DEM is the microscopic contact model. Previous studies have shown that the mechanical properties of MHBS are closely related to the temperature and pore pressure. In our previous studies, we have carried out a large number of micro-contact mechanical tests of two-dimensional(2D) ideal bonded particles[4-5], and proposed a 2D unified bond failure criterion[5], which is introduced into the discrete element program to simulate the mechanical properties of bonded granular systems[6]. Furthermore, the criterion of bond failure has been explored in depth[7]. On this basis, a 2D micro-contact model of MHBS considering the micro-characteristics of bonded MHBS is established[8]. In recent years, 3D bond failure criterion have been established by experimental tests[9] and numerical simulations of micro-contact mechanical properties of 3D ideal bonded particles, and 3D bond micro-contact model and grain-coating type micro-contact model of MHBS have been proposed[2,10]. However, the current model does not take into account the coupling effect between temperature, pore pressure and chemical conditions on the bond strength and stiffness of MH. This contributes to another strong motivation of this paper.

In this study, a thermo-hydro-mechanical-chemical (THMC) bond contact model which considers the influence of ambient temperature, pore pressure and chemical conditions, is proposed based on previous studies[4-5,7-10] to capture the microscopic contact behaviour of MHBS. This model based on the mechanical responses of the contact model in relation to environmental parameters, namely temperature T, pore pressure P, and salinity ω. A series of triaxial compression tests is simulated to investigate the mechanical properties of MHBS by DEM, where the simplified THMC bond contact model is implemented by the C++ code. In addition, the DEM simulation results are compared with the experimental data.

2 THMC BOND CONTACT MODEL FOR MHBS

2.1 Force-displacement Law

2.1.1 Particle contact

The force and moment can be calculated with the following formulas [11]:

$$\boldsymbol{F}_{\mathrm{n}}^{\mathrm{p}}=\begin{cases}k_{\mathrm{n}}^{\mathrm{p}}\boldsymbol{u}_{\mathrm{n}} & \boldsymbol{u}_{\mathrm{n}}\geq 0\\ \boldsymbol{0} & \boldsymbol{u}_{\mathrm{n}}<0\end{cases} \tag{1}$$

$$\boldsymbol{F}_{\mathrm{s}}^{\mathrm{p}}=\begin{cases}\left(\boldsymbol{F}_{\mathrm{s}}^{\mathrm{p}}\right)_{o}-k_{\mathrm{s}}^{\mathrm{p}}\Delta\boldsymbol{u}_{\mathrm{s}} & \boldsymbol{F}_{\mathrm{s}}^{\mathrm{p}}\leq\boldsymbol{F}_{\mathrm{s}}^{\max}\\ \boldsymbol{F}_{\mathrm{s}}^{\max}=\mu\boldsymbol{F}_{\mathrm{n}}^{\mathrm{p}} & \boldsymbol{F}_{\mathrm{s}}^{\mathrm{p}}>\boldsymbol{F}_{\mathrm{s}}^{\max}\end{cases} \tag{2}$$

$$\boldsymbol{M}_{\mathrm{r}}^{\mathrm{p}}=\begin{cases}k_{\mathrm{r}}^{\mathrm{p}}\Delta\boldsymbol{\theta}_{\mathrm{r}} & \boldsymbol{M}_{\mathrm{r}}^{\mathrm{p}}\leq\boldsymbol{M}_{\mathrm{r}}^{\max}\\ \boldsymbol{M}_{\mathrm{r}}^{\max}=0.25\zeta_{\mathrm{c}}\boldsymbol{F}_{\mathrm{n}}^{\mathrm{p}}\bar{R} & \boldsymbol{M}_{\mathrm{r}}^{\mathrm{p}}>\boldsymbol{M}_{\mathrm{r}}^{\max}\end{cases} \tag{3}$$

$$\boldsymbol{M}_{\mathrm{t}}^{\mathrm{p}}=\begin{cases}k_{\mathrm{t}}^{\mathrm{p}}\Delta\boldsymbol{\theta}_{\boldsymbol{t}} & \boldsymbol{M}_{\mathrm{t}}^{\mathrm{p}}\leq\boldsymbol{M}_{\mathrm{t}}^{\max}\\ \boldsymbol{M}_{\mathrm{t}}^{\max}=0.65\mu\boldsymbol{F}_{\mathrm{n}}^{\mathrm{p}}\bar{R} & \boldsymbol{M}_{\mathrm{t}}^{\mathrm{p}}>\boldsymbol{M}_{\mathrm{t}}^{\max}\end{cases} \tag{4}$$

where F_n^p, F_s^p, M_r^p and M_t^p denote the particle normal force due to compression, the particle tangential force due to relative displacement on the tangential plane, the particle moment due to rolling resistance and the torque due to twisting resistance, respectively. $k_n^p = 2RE_p$,$k_s^p = k_n^p/\xi$,$k_r^p = 0.25k_n^p\bar{R}^2$, $k_t^p = 0.5k_s^p\bar{R}^2$ are the normal, shear, bending and torsional stiffness, respectively, u_n is the overlap, $\left(F_s^p\right)_0$ is the tangential contact force in the previous step, μ is the inter-particle friction coefficient, $\zeta_c = 4.0$ is the parameter accounting for the local particle breakage. $\Delta u_s, \Delta\theta_r, \Delta\theta_t$ are the increments of the relative tangential displacement, bending angle and torsion angle in a time step, respectively.$\bar{R} = \beta R$ is the contact radius, where β is

the particle anti-rotation coefficient, $R = 2R_1R_2/(R_1 + R_2)$ is the equivalent radius . ξ=1.5 is the normal-to-shear stiffness ratio.

2.1.2 MH bond contact

The force and bending moment transmitted by cementation can be calculate using the following formula:

$$\boldsymbol{F}_{\mathrm{n}}^{\mathrm{b}} \leftarrow \boldsymbol{F}_{\mathrm{n}}^{\mathrm{b}} + k_{\mathrm{n}}^{\mathrm{b}} \boldsymbol{\Delta u}_{\mathrm{n}}^{\mathrm{b}} \tag{5}$$

$$\boldsymbol{F}_{\mathrm{s}}^{\mathrm{b}} \leftarrow \boldsymbol{F}_{\mathrm{s}}^{\mathrm{b}} + k_{\mathrm{s}}^{\mathrm{b}} \boldsymbol{\Delta u}_{\mathrm{s}}^{\mathrm{b}} \tag{6}$$

$$\boldsymbol{M}_{\mathrm{r}}^{\mathrm{b}} \leftarrow \boldsymbol{M}_{\mathrm{r}}^{\mathrm{b}} + k_{\mathrm{r}}^{\mathrm{b}} \boldsymbol{\Delta \theta}_{\mathrm{r}}^{\mathrm{b}} \tag{7}$$

$$\boldsymbol{M}_{\mathrm{t}}^{\mathrm{b}} \leftarrow \boldsymbol{M}_{\mathrm{t}}^{\mathrm{b}} + k_{\mathrm{t}}^{\mathrm{b}} \boldsymbol{\Delta \theta}_{\mathrm{t}}^{\mathrm{b}} \tag{8}$$

where F_n^b, F_s^b, M_r^b and M_t^b denote the normal force, shear force, bending moment and torsion moment of cementing contact respectively. k_n^b, k_s^b, k_r^b and k_t^b are the normal, tangential rolling and torsional stiffness of bond material[10]. Δu_n^b, Δu_s^b, $\Delta\theta_r^b$ and $\Delta\theta_t^b$ are the increments of the relative normal displacement, tangential displacement, bending angle and torsion angle of bond contact, respectively.

2.2 Bond failure criterion

The extension, compression, shear, bending and torsion strength of bond are calculated respectively according to the following formula[12]:

$$R_{\mathrm{nt}}^{\mathrm{b}} = \sigma_{\mathrm{t}} A_{\mathrm{b}} \tag{9}$$

$$R_{\mathrm{nc}}^{\mathrm{b}} = \sigma_{\mathrm{c}} A_{\mathrm{b}} \tag{10}$$

$$R_{\mathrm{s}}^{\mathrm{b}} = 0.145 \times \sqrt{\left(R_{\mathrm{nt}}^{\mathrm{b}} + R_{\mathrm{nc}}^{\mathrm{b}}\right)^2 - \left(2\boldsymbol{F}_{\mathrm{n}}^{\mathrm{b}} - R_{\mathrm{nc}}^{\mathrm{b}} + R_{\mathrm{nt}}^{\mathrm{b}}\right)^2} \tag{11}$$

$$R_{\mathrm{r}}^{\mathrm{b}} = 0.175 \times R_{\mathrm{b}} \times \sqrt{\left(R_{\mathrm{nt}}^{\mathrm{b}} + R_{\mathrm{nc}}^{\mathrm{b}}\right)^2 - \left(2\boldsymbol{F}_{\mathrm{n}}^{\mathrm{b}} - R_{\mathrm{nc}}^{\mathrm{b}} + R_{\mathrm{nt}}^{\mathrm{b}}\right)^2} \tag{12}$$

$$R_{\mathrm{t}}^{\mathrm{b}} = 0.189 \times R_{\mathrm{b}} \times \sqrt{\left(R_{\mathrm{nt}}^{\mathrm{b}} + R_{\mathrm{nc}}^{\mathrm{b}}\right)^2 - \left(2\boldsymbol{F}_{\mathrm{n}}^{\mathrm{b}} - R_{\mathrm{nc}}^{\mathrm{b}} + R_{\mathrm{nt}}^{\mathrm{b}}\right)^2} \tag{13}$$

where σ_t and σ_c are the tensile and compression strengths of bond material.R_{nt}^b , R_{nc}^b , R_s^b, R_r^b, R_t^b express peak tensile, compressive, shear, bending and torsional loads, respectively.

The bonded strength envelope is calculated by ellipsoid under composite load, which can be practically described as follows:

$$\left(\frac{\left\|\boldsymbol{F}_{\mathrm{s}}^{\mathrm{b}}\right\|}{R_{\mathrm{s}}^{\mathrm{b}}}\right)^2 + \left(\frac{\left\|\boldsymbol{M}_{\mathrm{r}}^{\mathrm{b}}\right\|}{R_{\mathrm{r}}^{\mathrm{b}}}\right)^2 + \left(\frac{\left\|\boldsymbol{M}_{\mathrm{t}}^{\mathrm{b}}\right\|}{R_{\mathrm{t}}^{\mathrm{b}}}\right)^2 \begin{cases} <1 & \text{Intact} \\ =1 & \text{Critical} \\ >1 & \text{Broken} \end{cases} \tag{14}$$

2.3 Bond Parameter determination based on temperature-pore-pressure-chemistry state

2.3.1 Thermal-hydro-mechanical effects

Hyodo et al.[13] showed that MH strength is strongly related to the temperature and pressure, and proposed a parameter *L* to represent the state of temperature and pressure. The parameter *L* is defined as the minimum distance between the normalized test condition point and the normalized stability boundary line.

Figure 1(a) summarised the relationship between the modified hydrate strength and the temperature and pressure parameter *L* in previous literatures[13-17]. It shows that a linear function $q_{\max} = 69.38 \times L$, can be used to fit the relationship the hydrate strength and the

temperature and pressure parameter L. It is worth mentioning that the compressive strength σ_c and tensile strength σ_t of hydrate can be modified as follows taking the backpressure σ_w into consideration:

$$\sigma_c = q_{max} = \sigma_{c,f} - \sigma_w = 69.38 \times L(\sigma_w, T) \tag{15}$$

$$\sigma_t = \sigma_w - \sigma_{t,f} = 69.38 \times L(\sigma_{t,f}, T) \tag{16}$$

where σ_{cf} is the major stress in compression failure and σ_{tf} is the major stress in tensile failure.

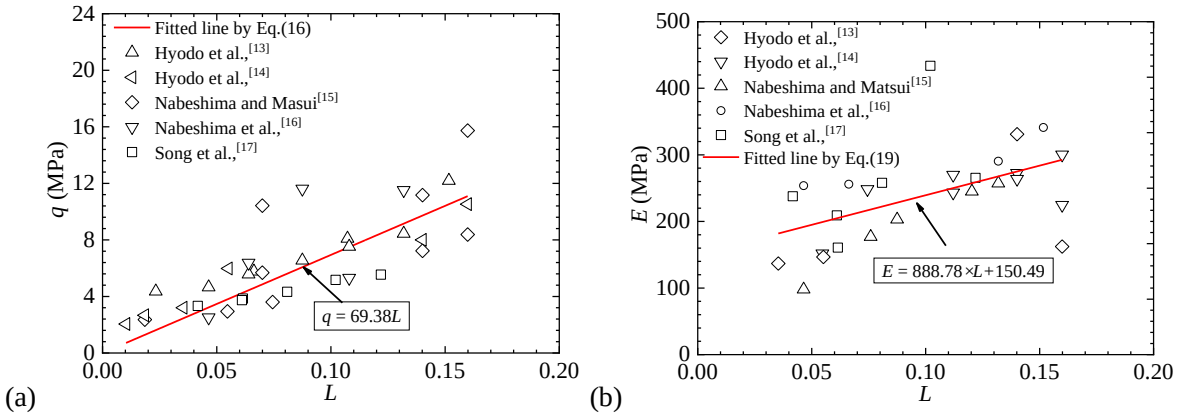

Figure 1: Relationship between methane hydrate strength/modulus and temperature and pressure parameters

Figure 1(b) provides the available experimental data of the elastic modulus of hydrate at different temperature and pressure[13-17]. It shows that the elastic modulus of hydrate can be expressed as follows:

$$E = 888.78 \times L + 150.49 \tag{17}$$

2.3.2 Chemical effects

It has been found that the chemicals such as NaCl can shit the MH phase equilibrium line, and thus results in the change of L. Figure 2 presents the data of phase equilibrium lines of hydrates in NaCl solutions of different concentrations form existing literatures[18-21]. The data can be divided into six series: 3wt%, 6wt%, 11wt%, 17wt%, 22wt% and 24wt%. It shows that with increase of slat solution, the hydrate temperature-pressure phase equilibrium line moves to the right slightly. Thus the parameter ω which characterizes chemical factors can be introduced into the MHBS model by fitting those data to establish the THMC bond contact model. The lower slope of methane hydrate on the right side of（T_0, P_0）in NaCl solution of different concentrations is assumed to be parallel to the temperature-pore-pressure equilibrium line of MH in pure water. The phase equilibrium line of MH at different salt solution can be summarized as Eq. (18):

$$\ln(P/P_0) = \begin{cases} -35 \times (T_0/T) + a & T \le T_0 \\ -7.5 \times (T_0/T) + b & T > T_0 \end{cases} \tag{18}$$

where the parameters a and b are the interceptions of the temperature and pressure phase equilibrium line of MH. Then, the effect of salinity ω can be introduced by the following equations:

$$a / a_0 = 0.00059 \times (w / w_0)^2 + 0.00253 \times (w / w_0) + 1 \tag{19}$$

$$b / b_0 = 0.00059 \times (w / w_0)^2 + 0.00253 \times (w / w_0) + 1 \tag{20}$$

where a_0=35 and b_0=7.5 are the interceptation of the equilibrium line of methane hydrate in pure water, respectively, and w_0 is the average salinity of seawater (w_0=3wt%).

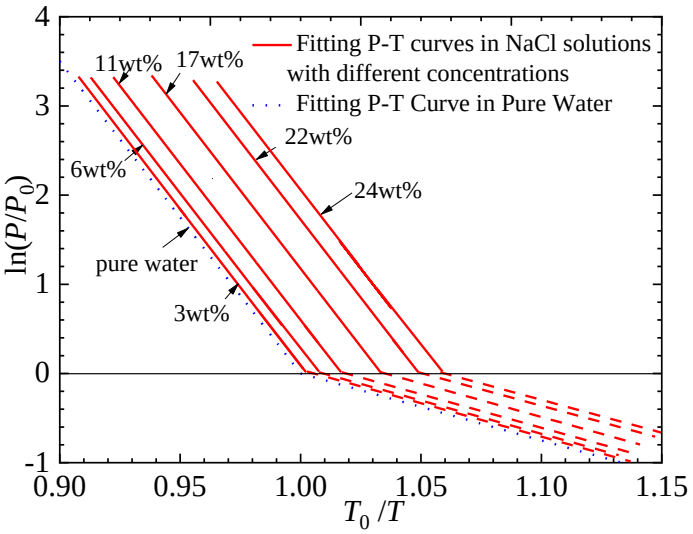

Figure 2: Phase equilibrium of hydrate in different concentration of salt solution

The whole area is divided into three areas as shown in figure 3. BD is the angle bisector seperating area I and II. In area I, line AB is used to caculate L while line BC is used in area II. In area III, MH would dissociate. Thus the test condition parameter L which is temperature, pressure and chemical dependent can be caculated using these equations

$$L=\begin{cases}\left|35\times\left(T_0/T\right)+\ln\left(P/P_0\right)-35\times\left[0.00059\times\left(w/w_0\right)^2+0.00253\times\left(w/w_0\right)+1\right]\right| \Big/ \sqrt{3.5^2+1^2} & \text{Zone I}\\ \left|7.5\times\left(T_0/T\right)+\ln\left(P/P_0\right)-7.5\times\left[0.00059\times\left(w/w_0\right)^2+0.00253\times\left(w/w_0\right)+1\right]\right| \Big/ \sqrt{7.5^2+1^2} & \text{Zone II}\\ 0 & \text{Zone III}\end{cases} \tag{21}$$

In the DEM simulation, the environmental parameters (temperature T, water pressure P and salinity ω) of the MHBS are input before hydrate formation. The position of the hydrate phase equilibrium line depends on the input environmental salinity, and the tensile strength, compressive strength and modulus of hydrate are determined by parameter L which depends on the temperature and water pressure.

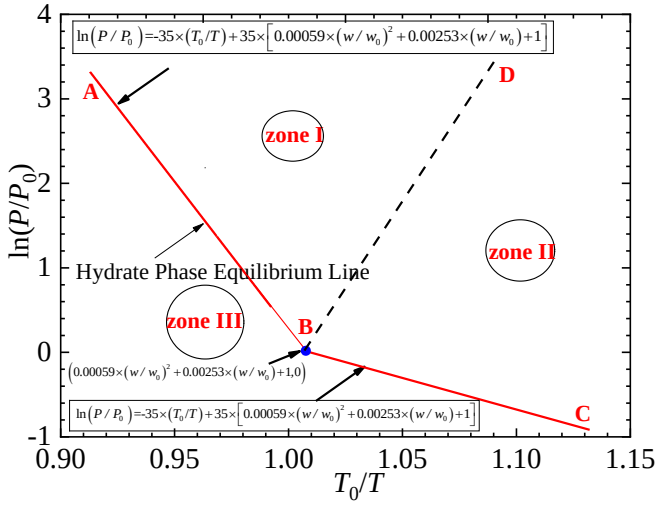

Figure 3: Equilibrium lines of hydrate phase and temperature and pressure conditions in the test

2.3.4 Parameters of contact model

The size of hydrate in real MHBS is much smaller than that in pure hydrate laboratory test. Since the strength of hydrate increases with the decrease of size, the tensile and compressive strength of hydrate was enlarged by 30 times in this study which can reflect the basic

characteristics of MHBS. The parameters in DEM simulations are shown in Table 1.

Table 1 Parameters of MHBS contact model

	Microscopic parameter of model	Numerical value
Particle contact	Particle modulus E_p (N/m^2)	7×10^8
	Particle normal tangential stiffness ratio ξ	5.0
	Particle anti-rotation coefficient β	0.25
	Particle local crushing coefficient ζc	4.0
	Coefficient of particle friction μ	0.5
MH Bond contact	Elastic modulus of hydrate E_b (N/m^2)	1.73×10^8
	Hydrate poisson ratio v_b	0.32
	Tensile strength of hydrate σ_t (N/m^2)	1.42×106×30
	Compressive strength of hydrate σ_c (N/m^2)	1.73×106×30
	Critical slenderness ratio of hydrate m_{cri}	0.05
	Hydrate radius multiplier λ	0.774/0.846/0.9
THMC parameter	Ambient temperature of the hydrate T (K)	278
	Hydrate environmental pressure P (MPa)	10
	Environmental salinity of hydrate w (wt%)	20/30/40

3 SIMULATION RESULTS

The triaxial compression tests were carried out under different hydrate saturations and effective confining pressures. The grain size distribution in our simulation is consistent with the Toyoura sand by Hyodo et al.[22], which ranges from 0.1 mm to 0.3 mm.

Figure 4(a) shows the stress-strain curves under different hydrate saturation. It can be seen that the presence of hydrate cementation can enhace the strain softening behavior, peak and residual shear strength signficantly, which is in good agreement with the laboratory tests[23]. Figure 4(b) presents the stress-strain behaviour of MHBS under different effective confining pressures (i.e 1MPa,3MPa,and 5MPa) and MH saturations (i.e. SMH=0%, SMH=40%) .The peak shear and residual shear stresses increase as the effective confining pressure increase at the same value of MH saturation. Under the same effective confining pressure, the peak shear stress increases and the subsequent softening behaviour is more obvious with increasing MH saturation.

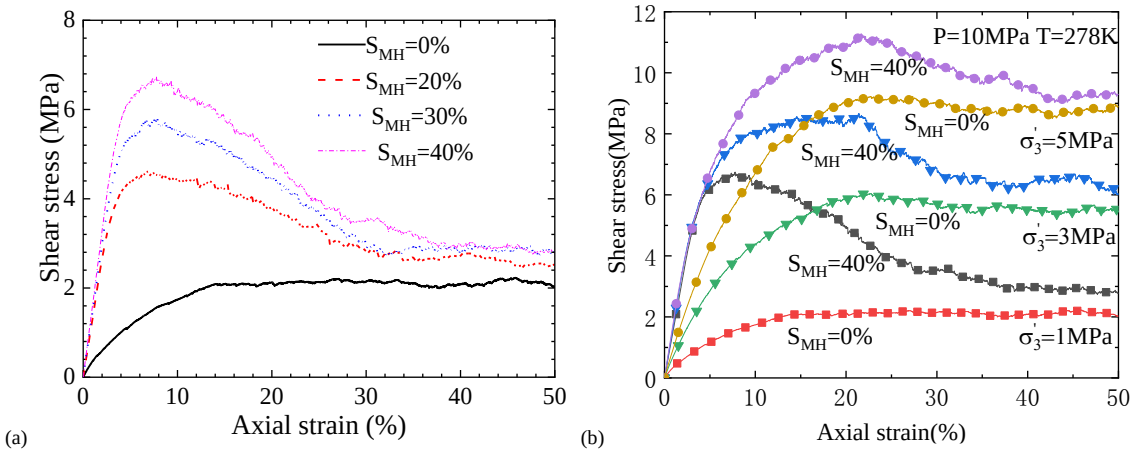

Figure 4: Stress and strain curves of MHBS under triaxial tests at different saturation/effective confining pressure

Figure 5 presents the stress-strain behaviour of MHBS under different NaCl concentrations (i.e 0wt%, 3wt%, 6wt%,and 10wt%). The higher the environmental salinity is, the more obvious the strain softening characteristics of the MHBS are. The peak shear strength decreases significantly with the increase of environmental salinity, while the residual shear strength decreases slightly with the increase of environmental salinity. When the residual state is reached, the residual strength is basically unchanged, but due to the presence of residual

hydrate, the residual strength is slightly higher than that of pure sand.

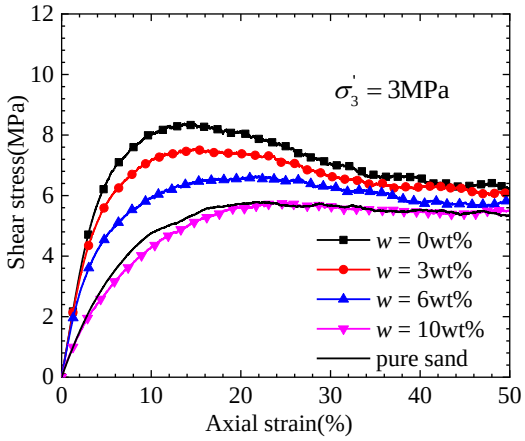

Figure 5: Stress and strain curves of MHBS under triaxial tests at different salinity

4 CONCLUSIONS

Based on the 3D bond contact model, considering the effect of ambient temperature, pressure and salinity on the tensile and compressive strength and modulus of cement, a 3D THMC micro-contact model of cemented MHBS is established. A series of triaxial tests are conducted to simulate the mechanical properties of MHBSs under different MH saturations and effective confining pressures by incorporating the simplified THMC bond model into the DEM. The results show that the DEM tests employing the 3D THMC contact model can capture the macroscopic mechanical behaviour of MHBS well, provides a basis for the following discrete element numerical study of macro-and micro- characteristics of MHBS.

Acknowledgements: The research was financially supported by the National Nature Science Foundation of China with Grant Nos.51639008, 51890911.

REFERENCES

[1] Soga, K., Lee, S.L., Ng, M.Y., and Klar, A. (2006) Characterisation and engineering properties of methane hydrate soils. *Characterisation and Engineering Properties of Natural Soils*, 4:2591-1642

[2] Shen Z.F, Jiang M.J. (2016) DEM simulation of bonded granular material. Part II: extension to grain-coating type methane hydrate bearing sand. *Computers and Geotechnics*, 75: 225-263.

[3] Cundall, P.A., Strack O.D.L. (1979). A discrete numerical model for granular assemblies. *Geotechnique* 29(1), 47-65.

[4] Jiang M.J, Sun Y.G, Xiao Y. (2012). An experimental investigation on the mechanical behavior between cemented granules. *Geotechnical Testing Journal*, 35(5): 678-690.

[5] Jiang M.J, Zhang N, Cui L, Jin S.L. (2015). A size-dependent bond failure criterion for cemented granules based on experimental studies. *Computers and Geotechnics*, 69: 182-198.

[6] Jiang M.J, Li T, Thornton C, Hu H.J. (2016). Wetting-induced collapse behavior of unsaturated and structural loess under biaxial tests using distinct element method. *International Journal of Geomechanics*, 17(1):06016010.

[7] Jiang M.J, Zhang F.G, Sun Y.G. (2014). An evaluation on the degradation evolutions in three constitutive models for bonded geomaterials by DEM analyses. *Computers and Geotechnics*, 57: 1-16.

[8] Jiang M.J, Zhu F.Y, Utili S. (2015). Investigation into the effect of backpressure on the

mechanical behavior of methane-hydrate-bearing sediments via DEM analyses. *Computers and Geotechnics*, 69: 551-563.

[9] Shen Z.F, Jiang M.J, Wan R. (2016). Numerical study of inter-particle bond failure by 3D discrete element method. *International Journal for Numerical and Analytical Methods in Geomechanics*, 40(4): 523-545.

[10] Shen Z.F, Jiang M.J, Thornton C. (2016b). DEM simulation of bonded granular material. Part I: contact model and application to cemented sand. *Computers and Geotechnics*, 75:192-209

[11] Jiang M.J, Shen Z.F, Wang J.F. (2015). A novel three-dimensional contact model for granulates incorporating rolling and twisting resistances. *Computers and Geotechnics*, 65: 147-163.

[12] Jiang M.J, Jin S.L, Coop M.R, Shen Z.F. (2019) A three-dimensional experimental study of inter-particle bond failure criterion. Acta Geotechnica, (under review)

[13] Hyodo M, Hyde A.F.L, Nakata Y, Yoshimoto N, Fukunaga M, Kubo K, Nanjo Y, Matsuo T. K. N. (2002). Triaxial compressive strength of methane hydrate *Proceedings of the Twelfth International Offshore and Polar Engineering Conference*, Kitakyushu, Japan, May 26-31, 422-428.

[14] Hyodo M, Nakata Y, Yoshimoto N, Ebinuma T. (2005). Basic research on the mechanical behavior of methane hydrate-sediments mixture. *Soils and Foundations*, 45(1): 75-85.

[15] Nabeshima Y, Matsui T. (2003). Static Shear Behaviors of Methane Hydrate and Ice. *The proceedings of the Fifth ISOPE Ocean Mining Symposium*: Tsukuba, Japan: exploration and survey, environment, mining systems and technology, processing technology, deep-ocean water upwelling, and gas hydrates, 156-158.

[16] Nabeshima Y, Takai Y, Komai T. (2005) Compressive Strength and Density of Methane Hydrate. *Proceedings of the Sixth ISOPE Ocean Mining Symposium*, Changsha, Hunan, China, October 9, 197-200.

[17] Song Y, Yu F, Li Y, Liu W, Zhao J. (2010). Mechanical property of artificial methane hydrate under triaxial compression. *Journal of Natural Gas Chemistry*, 19(3): 246-250.

[18] Dholabhai P, Englezos P, Kalogerakis N, Bishnoi P. (1991) Equilibrium conditions for methane hydrate formation in aqueous mixed electrolyte solutions. *The Canadian Journal of Chemical Engineering*, 69(3): 800-805.

[19] Jager M.D, Sloan E.D. (2001) The effect of pressure on methane hydration in pure water and sodium chloride solutions. *Fluid Phase Equilibria*, 185(1):89-99.

[20] Lafond P.G, Olcott K.A, Sloan E.D, Koh C.A, Sum A.K. (2012) Measurements of methane hydrate equilibrium in systems inhibited with NaCl and methanol. *Journal of Chemical Thermodynamic*s, 48: 1-6.

[21] Cha M, Hu Y, Sum A.K. (2016) Methane hydrate phase equilibria for systems containing NaCl, KCl, and NH4Cl. *Fluid Phase Equilibria*, 413: 2-9.

[22] Hyodo M, Yoneda J, Yoshimoto N, Nakata Y. (2013). Mechanical and dissociation properties of methane hydrate-bearing sand in deep seabed. *Soils and Foundations*, 53(2): 299-314.

[23] Masui A, Haneda H, Ogata Y, Aoki K. (2005). Effects of methane hydrate formation on shear strength of synthetic methane hydrate sediments. *Proceedings of The 15th International Offshore and Polar Engineering Conference*, Seoul, Korea, 19-24.